GeV Electron Beams from a Capillary Discharge Guided Laser Plasma Accelerator*

K. Nakamura, A. J. Gonsalves, D. Panasenko, C. Lin,
C. Toth, C. G. R. Geddes, C. B. Schroeder, E. Esarey, and W. P. Leemans†,
LBNL, Berkeley, CA 94720, USA

Abstract

Laser plasma acceleration (LPA) up to 1 GeV has been realized at Lawrence Berkeley National Laboratory by using a capillary discharge waveguide. In this paper, the capillary discharge guided LPA system including a broadband single-shot electron spectrometer is described. The spectrometer was designed specifically for LPA experiments and has a momentum acceptance of 0.01 – 1.1 GeV/c with a percent level resolution. Experiments using a 33 mm long, 300 μm diameter capillary demonstrated the generation of high energy electron beams up to 1 GeV. By de-tuning discharge delay from optimum guiding performance, self-trapping and acceleration were found to be stabilized producing 460 MeV electron beams.

INTRODUCTION

Laser plasma accelerators (LPAs) [1] have demonstrated their capability of sustaining accelerating gradients up to several hundred GV/m, which makes them attractive as compact particle accelerators or radiation sources. Furthermore, the intrinsically laser-synchronized electron beams (e-beams) are naturally short in time duration because the characteristic scale length of the accelerating structure is the plasma wavelength, which is typically $\sim$ 10 μm ($\sim$ 30 fs). The LPA offers ways to realize many kinds of femto second pump-probe experiments, which may be of benefit to ultra-fast sciences.

One of the main goals in the present LPA research is to increase the energy with improved stability and tunability. The energy is a key parameter when applications such as light sources are considered. In 2004, a breakthrough was reported with the generation of high quality 100 MeV class e-beams from LPAs [2, 3, 4], while the conventional light sources consist of accelerators that provide up to several GeV. The stability and tunability are of great interest for all kind of applications.

In the LOASIS Program at Lawrence Berkeley National Laboratory (LBNL), to pursue those frontiers, a new kind of LPA was designed. Instead of a gas jet target, a hydrogen-filled capillary discharge waveguide [5, 6] was used. In this scheme, intense laer pulses were guided over a distance 10 times the Rayleigh range by a preformed plasma channel with sufficiently low density plasma to reduce energy gain limitation imposed by diffraction and dephasing [1]. In 2006, experiments using a 33 mm long, 310 μm diameter capillary demonstrated the generation of high energy e-beams up to 1 GeV [7, 8]. Critical to the GeV-class capillary discharge guided (CDG) LPA was the development of a diagnostic for the e-beam, namely an electron spectrometer (ESM) [9]. In this paper, the CDG-LPA system including a broadband single-shot electron spectrometer is described, and a performance analysis of the recent experiments using a 33 mm long, 300 μm diameter and a 15 mm long, 200 μm diameter capillary is reported. Experiments varying capillary length give insight into the physics of the capillary discharge guided LPA, and provide essential information for the design of the next generation apparatus [10].

EXPERIMENTAL SETUP

The schematic of the experimental setup is shown in Fig. 1. The laser that was utilized was the TREX arm of the 10 Hz Ti:Al_2O_3 system of the LOASIS facility at LBNL. The laser beam was focused by a f/25 off-axis parabolic mirror providing a typical focal spot size of $r_0 \simeq 25$ μm that contains 60% of the laser energy. Here, a Gaussian transverse profile of $I = I_0 \exp(-2r^2/r_0^2)$ is assumed. Full energy and optimum compression gives $P = 43$ TW, $\tau_{in} \simeq 40$ fs full width half maximum (FWHM) intensity, calculated peak intensity $I_0 = 2P/\pi r_0^2 \simeq 2.6 \times 10^{18}$ W/cm^2, and a normalized vector potential $a_0 \simeq 8.6 \times 10^{-10}\lambda[\mu\mathrm{m}]I^{1/2}[\mathrm{W/cm^2}] \simeq 1.1$. The capillary waveguide was laser-machined in sapphire plates. Hydrogen gas was introduced into the capillary using two gas slots as shown in Fig. 1(inset). A discharge was struck between electrodes located at each end of the waveguide, using a high voltage pulsed power supply with a 4 nF capacitor charged to between 15 and 22 kV. Measurements showed that a fully ionized, approximately parabolic channel was formed on axis [6]. This fully ionized feature was also confirmed by the absence of ionization induced blueshifting of the transmitted laser spectrum when a low power (< 0.2 TW) laser pulse was guided. The laser energy was monitored both before and after the interaction to evaluate the guiding efficiency and guided beam quality. The laser output spectrum was measured by a broadband optical spectrometer which covers a wavelength range of 320 to 1000 nm in a single shot.

The e-beams generated were characterized by an electron spectrometer. The electron spectrometer utilized a water-cooled round dipole electro-magnet Varian 4012A, which had a 65 mm gap and was powered by a Glass-

* Work supported by DOE grant DE-AC02-05CH11231, and DARPA
† wpleemans@lbl.gov

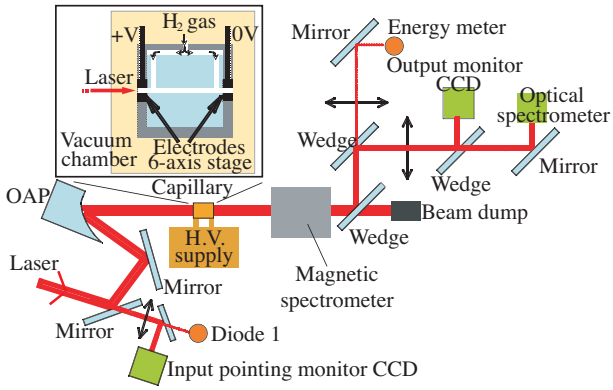

Figure 1: Schematic diagram of the capillary discharge-guided laser wakefield accelerator and diagnostics. The detailed description of the capillary discharge unit is in the upper inset. See manuscript for detailed information of the magnetic spectrometer.

man SH3R2.7 power supply. The magnetic spectrometer allowed simultaneous measurement of the laser pulse and e-beam due to its large gap. The magnetic field was measured by a Hall probe along the mid-plane, and the effective radius, defined by $R_{eff} = [\int_0^\infty B_x(r)dr]/B_x(0)$, was found to be 195 mm with peak field $B_x(0) = 1.25$ T. The magnet deflected the electrons vertically downward onto two scintillating screens (LANEX Fast Back from Kodak) mounted on the exit flanges of the vacuum chamber. Four synchronously triggered 12-bit charge-coupled device (CCD) cameras (model Flea from Point grey research) imaged a 75 cm long (bottom) and a 45 cm long (forward) screens with F number 1.4 – focal length 4.8 to 6.4 mm video lenses, allowing simultaneous single shot measurement of electrons from 0.01 GeV to 0.14 GeV (bottom) and 0.17 GeV to 1.1 GeV (forward) with a peak magnetic field of 1.25 T. Spatial resolutions of those CCD cameras were measured to be $0.6 - 1$ mm for the forward screen and $\simeq 2.5$ mm for the bottom screen. Stray laser light was blocked by $\simeq 40$ μm thick aluminum foil on the back of the screens. In addition, bandpass filters [central wavelength 550 nm, width 70 nm full-width half-maximum (FWHM)] were installed in front of each CCD camera to separate green fluorescent light from the intense infrared laser light. To avoid electrons from hitting the CCD cameras directly, first-surface mirrors were used at 45° following the exit flanges, which separated fluorescent light from the electrons.

The imaging properties of the spectrometer were determined via the edge focusing. The displacement of the dipole magnet center with respect to the laser propagation axis was carefully chosen to provide the necessary edge focusing. One can achieve the minimum energy resolution and error in the determination of the absolute energy by observing e-beams at the foci in the dispersive plane. By having the laser propagation axis below (above) the magnet center, the edges provide converging (diverging) power in the dispersive plane, and diverging (converging) power in the non-dispersive plane. The stronger converging power in the dispersive plane provides a more compact system because the foci in the dispersive plane are closer to the magnet, while it results in a smaller angular acceptance due to the stronger diverging power in the non-dispersive plane. High energy e-beams become somewhat insensitive to edge focusing due to their rigidity, and their resolutions are determined mostly by their angular divergence. For observation of high energy e-beams, the forward view was arranged to achieve the desirable angular acceptance and system dimensions. The laser propagation axis was placed 25.4 mm below the magnet center to achieve desirable foci arrangement for the dispersive plane and reasonable angular acceptance. Note that the imaging (focusing) was achieved only in the dispersive plane. The bottom view was arranged (30 degree downward from the laser propagation axis) to observe e-beams as close to the calculated first-order foci in the dispersive plane as possible.

In order for a performance evaluation, the electron trajectories on the mid-plane (reference trajectories) were computed by calculating the deflection angle based on the Lorentz force. The input midplane field was generated through a 2D interpolation of the measured field profile along the radial axis. For each trajectory, the 6-dimensional e-beam properties were calculated by using the arbitrary-order beam dynamics code COSY INFINITY (COSY) [11]. Due to the collimator-free scheme, the measured momentum resolution contained a contribution from the e-beam divergence, which depended on the accelerator configuration and parameters such as the laser energy or the capillary length and diameter. As a result, the e-beam divergence showed shot-to-shot fluctuations. Therefore, the momentum resolution and the energy spread were evaluated for each shot with the following procedure. From the computed imaging properties, the horizontal beam divergence $\sigma_{x'0}$ was calculated from the measured horizontal beam size σ_{x1} with a given beam size at the source, σ_{x0} and σ_{y0}, which were assumed to be the same size as the laser output mode size. The effect of the source size on the image was almost negligible since the beam size at the source was smaller by an order of magnitude than the typical product of beam divergence and propagation distance. By assuming an axisymmetric e-beam profile (i.e., equal horizontal and vertical divergence), the vertical beam divergence $\sigma_{y'0} = \sigma_{x'0}$ was obtained and used to calculate the vertical beam size at the screen with a specific central energy and zero energy spread, σ_{y1mono}. The image size gave the intrinsic resolution of the ESM, δE_{mono}. The real energy spread of an e-beam δE_{beam} was then calculated by deconvolving the effect of finite divergence from the measured e-beam profile δE_{img} using $\delta E_{img} = \sqrt{\delta E_{beam}^2 + \delta E_{mono}^2}$. The momentum resolutions for $\sigma_{x'0} = \sigma_{y'0} = 1$ and 2 mrad e-beams are shown in Fig. 2, where the beam profile was assumed to be a Gaussian distribution with $\sigma_{x0} = \sigma_{y0} = 20$ μm. The momentum resolution is below 2% (4%) for a 1 mrad (2 mrad)

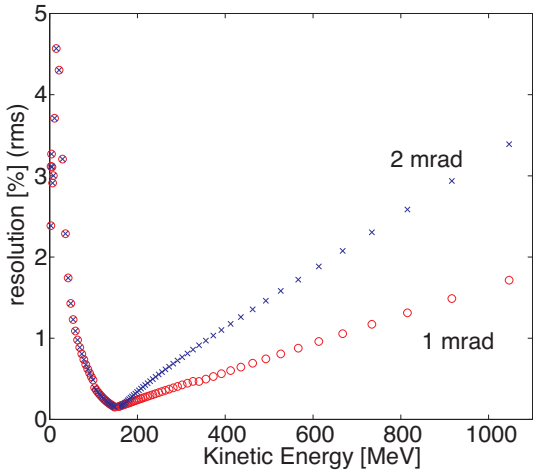

Figure 2: Momentum resolutions for $\sigma_{x'0} = \sigma_{y'0} = 1$ and 2 mrad electron beams. Horizontal axis is the kinetic energy of the electron beam for a peak magnetic field of 1.25 T. The input beam size was assumed to be a Gaussian distribution with $\sigma_{x0} = \sigma_{y0} = 20$ μm.

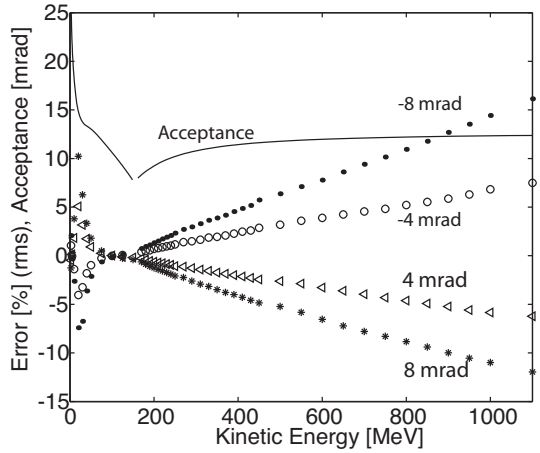

Figure 3: Errors in the determination of the absolute energy for angles ranging from -8 mrad to +8 mrad. Horizontal axis is the kinetic energy of the electron beam for a peak magnetic field of 1.25 T. The geometrical acceptance of the spectrometer is also shown (solid line).

divergence beam in the energy range of the ESM.

The collimator-free scheme also introduced an uncertainty in the determination of the absolute energy. The energy of an e-beam with positive (negative) incident angle in vertical axis would be measured higher (lower) than the actual energy. The errors in the determination of the energy of electrons with certain incident angle (± 4 and ± 8 mrad) were computed and shown in Fig. 3, where the magnetic field was taken to be 1.25 T. For example, the e-beam measured as 1.0 GeV might have been 0.94 (1.07) GeV with a 0.4 (-0.4) mrad incident angle. The fluctuation level in the incident angle in the vertical plane was evaluated as follows. From the measured beam position in the horizontal plane x_{1peak}, the angular fluctuation in the horizontal plane σ_{x1peak} (rms) was statistically evaluated. With the assumption of symmetric behavior in both planes $\sigma_{y1peak} = \sigma_{x1peak}$, the fluctuations in the incident angle in the vertical plane were then determined. The angular fluctuations showed a dependence on the accelerator configuration (e.g., the laser energy or the capillary length and diameter), and the typical value was found to be 2 to 6 mrad (1σ), which gave $\sim 3\%$ to 11% error at 1.0 GeV, or $\sim 1\%$ to 5% error at 0.5 GeV. Also shown in Fig. 3 is the geometrical acceptance. The acceptance was trajectory dependent due to the differences in the path length and the imaging properties. More than ± 10 mrad acceptance was achieved in most of the energy range.

The total number of electrons was obtained from the intensity on the scintillating screen, which was cross-calibrated against an integrating current transformer (ICT) at the Advanced Light Source (ALS), LBNL [12]. By using an energy tunable (0.071 GeV to 1.2 GeV), 20 ps long (root-mean-square, rms) e-beams, the intensity - number of electrons calibration was performed for an identical CCD camera and scintillating screen over a broad range of the electron energy. The sensitivity difference between the CCD cameras due to the different screen-camera distance was taken into account by using a LED source to cross-calibrate. Note that since the instantaneous intensity of the ALS e-beams [2.0 pC/(ps mm^2) on the screen] was not as high as that of typical LPAs, there is a possibility that the ALS calibration underestimated beam charge due to the saturation of the scintillating screen caused by the high instantaneous intensity of the e-beam.

RESULTS

In 2006, generation of e-beams with energies of 1 GeV was reported for a 33 mm long, 300 μm diameter capillary with three gas slots [7, 8]. Similarly to these results, a parameter regime where e-beams with energies of up to 1 GeV were produced was found here for a 33 mm long, 300 μm diameter capillary with two gas slots. Representative single shot e-beam spectra are shown in Fig. 4(a)-(c). The plasma density was $n_0 \sim 5.3 \times 10^{18}$ cm^{-3}, the laser parameters were 1.5 J (86 mJ rms), 46 fs ($a_0 \sim 0.93$), applied voltage was 18 kV, and the discharge delay was $t_d \sim 580$ ns. In this parameter regime, 51 shots were taken, and 37 shots produced electrons above 400 MeV. The mean peak energy was 713 MeV, and mean charge was 6 pC. Since e-beams were often observed with a low energy tail in this regime, electrons with energy above 400 MeV were taken into account for the analysis. The mean laser transmission was 65%.

The peak energy and maximum energy versus total charge for 33 mm long, 300 μm diameter capillary are shown in Fig. 4(d). The peak energy showed clear dependence on the charge, while the maximum energy was somewhat insensitive to charge. There are several possible

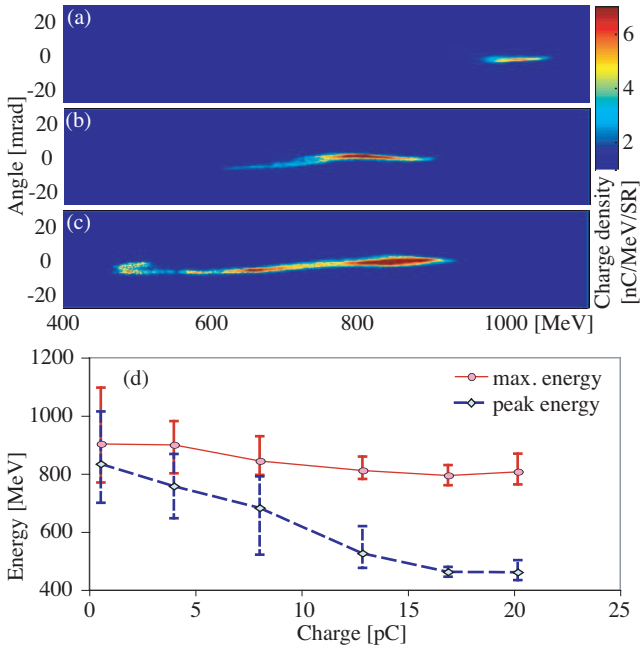

Figure 4: (a)-(c) Representative single shot e-beam spectra, (d) the peak energy and maximum energy versus charge for the 33 mm long, 300 μm diameter capillary. (The plasma density was $\sim 5.3 \times 10^{18}$ cm^{-3}, the laser was 1.5 J–46 fs, the applied voltage was 18 kV, and the discharge delay was $\sim$ 580 ns.)

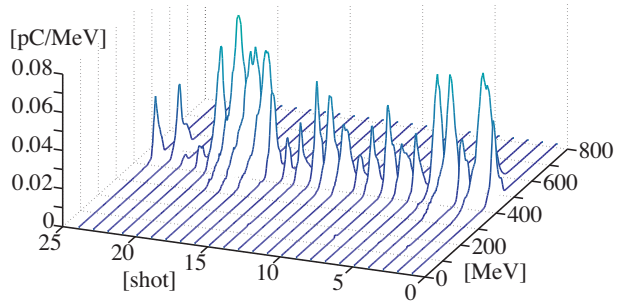

Figure 5: Single shot spectra of 24 consecutive shots for the 33 mm long, 300 μm diameter capillary. (The plasma density was $\sim 3.4 \times 10^{18}$ cm^{-3}, the laser was 1.5 J –46 fs, the applied voltage was 25 kV, and the discharge delay was $\sim$ 680 ns.)

scenarios. The trapped e-beam produces a wakefield which can partly cancel the wakefield generated by the laser pulse (beam loading effect). In the case of heavy beam loading, self-trapping can be stopped, and the tail of the e-beam sees a lower accelerating field while the head sees the maximum field, introducing energy spread to the e-beam. If beam loading is negligible, self-trapping can occur over a longer period of time, and these higher charge beams may be trapped over a larger phase region in the plasma wave, resulting in a larger energy spread. To produce high quality e-beams in a reproducible manner, controlling the amount, duration, and the location of trapped electrons will be critical.

Also found with this capillary was stable generation of quasi-monoenergetic 460 MeV beams (shown in Fig. 5) for plasma density $n_0 \sim 3.4 \times 10^{18}$ cm^{-3}, and laser parameters 1.5 J (36 mJ rms), 46 fs ($a_0 \sim 0.93$). The applied voltage was 25 kV, and the discharge delay $t_d \sim 680$ ns (with 0.9 ns rms jitter). In this parameter regime, 24 shots were taken, and all 24 shots produced electrons with mean charge 2.6 pC (2.0 pC rms), mean peak energy 458 MeV (24 MeV rms), and mean energy spread 4% rms. Applying longer discharge delay and higher voltage than the high energy regime resulted in stabilizing self-trapping and acceleration to somewhat lower electron energy.

In experiments using a 15 mm long, 200 μm diameter capillary, the guiding performance and e-beam generation showed clear dependence on the discharge delay. The input laser parameters were 0.9 J (36 mJ rms), 41 fs ($a_0 \sim 0.8$), and the plasma density was 2.5 or 3.7 $\times 10^{18}$ cm^{-3}. Shown in Fig. 6(a) are the discharge delay dependence of several laser spectra bins. The center is defined as the light within the frequency bandwidth of $770 \leq \lambda \leq 835$ nm, and 100% of incident light was within this band. The red (blue) shift is defined as $835 < \lambda < 1000$ nm ($320 < \lambda < 770$ nm). For relatively short discharge delay ($t_d < 130$ ns), significant red-shift and moderate blue-shift were observed, consistent with the laser pulse modulation and energy deposition onto the plasma via wakefield generation [1]. For longer discharge delay ($t_d > 130$ ns), the optical spectrum exhibited significant blue-shift as well as red-shift, and the transmission efficiency dropped.

The probability of observing any e-beam on the electron spectrometer vs. t_d is shown in Fig. 6(b) by dashed lines. For $n_0 \sim 2.5 \times 10^{18}$ cm^{-3}, no e-beams were observed for $t_d < 110$ ns and transmission efficiency was high (> 80%). This suggests that, although a wakefield was generated based on the observation of significant red-shift, it was not large enough to trap background electrons. Electron beams were observed for longer discharge delay, along with a drop in transmission efficiency and enhanced blue-shift. For e-beam properties, relatively high energy (~ 300 MeV), low charge (< 10 pC) quasi-monoenergetic e-beams were observed with shorter discharge delay while broadband high charge ($\sim$100 pC) beams were observed with longer delay. Note that by using higher density plasma ($n_0 \sim 3.7 \times 10^{18}$ cm^{-3}), e-beams were observed for shorter discharge delay without significant blue shift in transmitted optical spectrum.

Several mechanisms could be responsible for the enhancement of blueshifting, laser transmission loss, and electron trapping observed for longer discharge delay. For longer discharge delay, the degree of ionization, depth of the plasma channel, and plasma density decrease. It has also been suggested that the amount of discharge-ablated material interacting with the laser pulse increased [13]. For a substantial amount of laser pulse energy to be blueshifted by ionization requires the peak intensity of the laser pulse

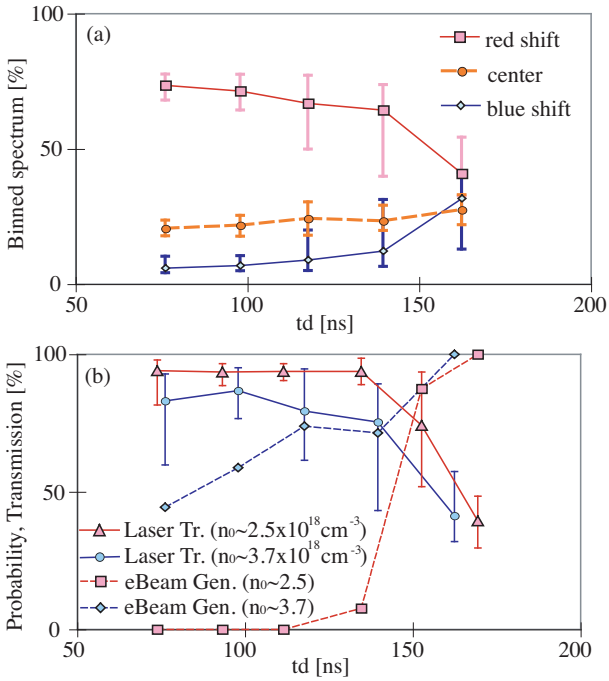

Figure 6: Results for 15 mm long, 200 μm diameter capillary. (a) Binned transmitted optical spectrum versus discharge delay for plasma density $\sim 2.5 \times 10^{18}$ cm^{-3}. The center is defined as the light within the frequency bandwidth of $770 \leq \lambda \leq 835$ nm. The red (blue) shift is defined as $835 < \lambda < 1000$ nm ($320 < \lambda < 770$ nm). (b) Transmission efficiency of laser pulses [solid line, triangles (circles) for $n_0 \sim 2.5(3.7) \times 10^{18}$ cm^{-3}], and the probability of e-beam observation on the electron spectrometer [dashed line, squares (diamonds) for $n_0 \sim 2.5(3.7) \times 10^{18}$ cm^{-3}] versus discharge delay. For both figures, the laser was 0.9 J–41 fs. A total of 80 shots were taken for each plasma density. Bars show minimum and maximum points.

to be within an order of magnitude of the ionization intensity of the ion species with which the pulse interacts. In the case of hydrogen this is $10^{14} - 10^{15}$ W/cm^2, several orders of magnitude lower than the intensity of the laser in the channel. Ablated materials (e.g., aluminum, oxygen) have higher ionization thresholds, and the deteriorated channel may lead to laser ablation of the capillary wall. The reduced laser transmission was likely due to ionization and/or laser leakage from the degraded channel. A recent study also suggested the interaction with a partially ionized plasma could assist self-trapping [14, 15]. Discharge-ablated materials drifting to the axis before the arrival of the laser could contribute to this process due to its transit time. Note that laser-ablated materials could not contribute to this process. Another possible reason for increased trapping is increase of the on-axis plasma density due to the deterioration of the channel. Although the degree of ionization decreases for longer discharge delay, the laser pulse was strong enough to ionize hydrogen.

SUMMARY

In summary, the capillary discharge guided laser plasma accelerator (CDG-LPA) system including the broadband single-shot electron spectrometer was described. The ESM has the momentum acceptance of 0.01 – 1.1 GeV/c with a percent level resolution. Relativistic e-beam generation via a CDG-LPA was studied by using 15 mm long, 200 μm diameter and 33 mm long, 300 μm diameter capillaries. Generation of quasi-monoenergetic e-beams up to 1 GeV was observed from the the 33 mm long capillary, and up to 300 MeV was observed from the 15 mm long capillary. By using longer discharge delay, self-trapping was stabilized. This regime could be used to design a stable self injection CDG-LPA. While reproducible beams have been observed in tightly controlled parameter regime, a controlled mechanism for injection will be important to enhance the LPA performance, such as longitudinal density tailoring [10].

REFERENCES

[1] E. Esarey, P. Sprangle, J. Krall, and A. Ting. *IEEE Trans. Plasma Sci.*, 24(2):252–288, 1996.

[2] S. P .D. Mangles, *et al.*, *Nature*, 431:535–538, 2004.

[3] C. G. R. Geddes, Cs. Tóth, J. van Tilborg, E. Esarey, C. B. Schroeder, D. Bruhwiler, C. Nieter, J. Cary, and W. P. Leemans. *Nature*, 431:538–541, 2004.

[4] J. Faure, Y. Glinec, A. Pukhov, S. Kiselev, S. Gordienko, E. Lefebvre, J.-P. Rousseau, F. Burgy, and V. Malka. *Nature*, 431:541–544, 2004.

[5] D. J. Spence and S. M. Hooker. *Phys. Rev. E*, 63(1):015401, 2000.

[6] A. J. Gonsalves, T. P. Rowlands-Rees, B. H. P. Broks, J. J. A. M. van der Mullen, and S. M. Hooker. *Phys. Rev. Lett.*, 98:025002, 2007.

[7] W. P. Leemans, B. Nagler, A. J. Gonsalves, Cs. Tóth, K. Nakamura, C. G. R. Geddes, E. Esarey, C. B. Schroeder, and S. M. Hooker. *Nature Physics*, 2:696–699, 2006.

[8] K. Nakamura, B. Nagler, Cs. Tóth, C. G. R. Geddes, C. B. Schroeder, E. Esarey, W. P. Leemans, A. J. Gonsalves, and S. M. Hooker. *Physics of Plasmas*, 14(5):056708, 2007.

[9] K. Nakamura, W. Wang, N. Ybarrolaza, D. Syversrud, J. Wallig, and W.P. Leemans. *Rev. Sci. Instrum.*, 79:053301, 2008.

[10] A. J. Gonsalves, E. Esarey, C. G. R. Geddes, W. P. Leemans, C. Lin, K. Nakamura, D. Panasenko, C. B. Schroeder, and C. Toth. In *Proceedings of the 2009 Particle Accelerator Conference*, Piscataway, NJ, 2009. IEEE.

[11] K. Makino and M. Berz. *Nucl. Instrum. Methods Phys. Res. A*, 427:338, 1999.

[12] K. Nakamura. in preparation.

[13] A. J. Gonsalves. PhD thesis, University of Oxford, 2006.

[14] E. Oz, *et al.*, *Phys. Rev. Lett.*, 98(8):084801, 2007.

[15] T. P. Rowlands-Rees, *et al.*, *Phys. Rev. Lett.*, 100:105005, 2008.